Combined remote mineralogical and elemental identification from rovers: Field and laboratory tests using reflectance and laser-induced breakdown spectroscopy

Roger C. Wiens,[1] Raymond E. Arvidson,[2] David A. Cremers,[3] Monty J. Ferris,[3] James D. Blacic,[4] Frank P. Seelos IV,[2] and Kim S. Deal[2]

Received 1 December 2000; revised 2 November 2001; accepted 20 November 2001; published XX Month 2002.

[1] Rover mast-based stereo imaging, reflectance or emission spectra, and laser-induced breakdown spectroscopy (LIBS) will provide powerful synergistic data sets for rapidly determining geologic setting, mineralogy, and elemental composition for rock and soil targets. We report results from hand specimen examination, multiple spectral reflectance (VISIR, 0.4–2.5 μm), and remote LIBS measurements for representative samples (basalt, iron oxides, altered rhyolite, and dolostone) collected during the May 2000 rover trials at Black Rock Summit, Nevada. Major findings are (1) reflectance data indicate the presence of olivine and montmorillonite for the basaltic sample, whereas LIBS data show variations with depth as an alumino-silicate coating is ablated and a basaltic composition is revealed beneath; (2) iron oxide reflectance data are dominated by goethite and hematite with the additional detection of hydrated cryptocrystalline SiO_2 (an interpretation fully supported by the LIBS data); (3) VISIR reflectance data for rhyolite show significant alteration to kaolinite, an inference that would be difficult to make from LIBS data alone; (4) dolostone reflectance data show dominantly dolomite with minor iron oxides, inferences confirmed through analyses of LIBS data; and (5) LIBS data acquired for samples as a function of depth and spatial location significantly aid in understanding the extent of sample coatings and compositional and mineralogical diversity. Given the hand specimen examination and results from joint analysis of the two rapid-acquisition spectral techniques, a scenario for acquisition and analysis of mast-based imaging reflectance or emission spectroscopy and LIBS is presented within the context of the scientific objectives for the Mars Exploration Program. *INDEX TERMS:* 1094 Geochemistry: Instruments and techniques; 1060 Geochemistry: Planetary geochemistry (5405, 5410, 5704, 5709, 6005, 6008); 6225 Planetology: Solar System Objects: Mars; 5494 Planetology: Solid Surface Planets: Instruments and techniques; *KEYWORDS:* Laser-induced breakdown spectroscopy (LIBS), Mars chemistry, major elements, rover, spectroscopy, VIS-IR, LIBS

1. Introduction

[2] Planetary rovers have provided and will continue to provide the mobility needed to explore terrains using remote sensing, conduct in situ analyses of samples, and enable the detailed measurements needed to complement orbital observations [*Golombek et al.*, 1997]. For example, the two Mars Exploration Rovers (MER-A, MER-B) to be launched as part of the Mars Surveyor Program in 2003 will each conduct remote-sensing and in situ measurements over distances of up to 1 km during their 90 sol primary missions. In this article we report on the joint, synergistic use of hand specimen descriptions combined with two remote-sensing techniques to acquire textural, mineralogical, and chemical information about soils and rocks during rover traverses. The techniques implemented in this study include visual examination of samples, visible and infrared (VISIR) reflectance, and laser-induced breakdown spectroscopy (LIBS). These measurements of the same targets can be acquired from stand-off distances of several meters followed by close-up imaging to provide detailed textural information. VISIR and LIBS techniques are shown to circumvent key limitations of past, scheduled, and contemplated rover payloads. Specifically, the Pathfinder Alpha Proton X-ray Spectrometer (APXS) [*Reider et al.*, 1997] and the similar system planned for MERs require detailed placement of the instrument onto the target and integration times of many hours to acquire elemental abundance data. The combined use of VISIR/LIBS can be done remotely from a rover at a stand-off

[1]Space and Atmospheric Sciences, Los Alamos National Laboratory, Los Alamos, New Mexico, USA.
[2]Department of Earth and Planetary Sciences, McDonnell Center for the Space Sciences, Washington University, St. Louis, Missouri, USA.
[3]Chemistry Division, Los Alamos National Laboratory, Los Alamos, New Mexico, USA.
[4]Earth and Environmental Sciences, Los Alamos National Laboratory, Los Alamos, New Mexico, USA.

0148-0227/02/2000JE001439$09.00

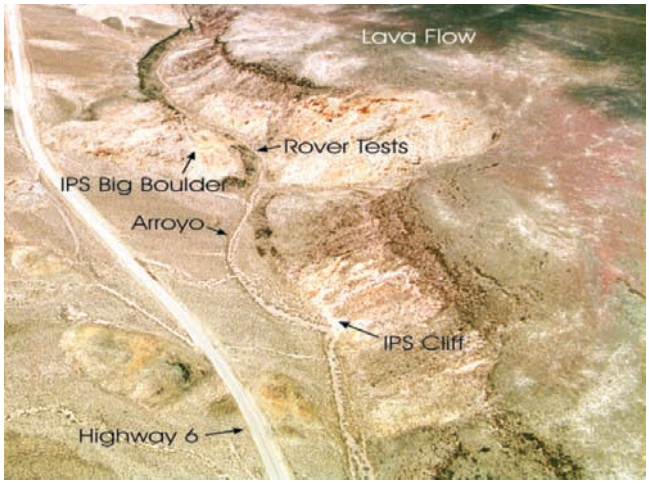

Figure 1. Overhead photograph showing the field site and major outcrops at Black Rock Summit for the K9 and FIDO experiments conducted in May 2000. North is to the upper right corner of the image.

distance of several meters using azimuth and elevation actuators to point the instruments. Integration times are only minutes rather than many hours. When combined with mast-based stereo and close-up imaging, the use of reflectance and/or emission spectroscopy and LIBS will prove to be powerful indeed. Further, dust coatings have been shown to significantly affect APXS results from the Pathfinder site [e.g., *McSween et al.*, 1999]. LIBS can be used as an ablation tool to remove dust or thin weathering coatings and thus acquire elemental abundance data as a function of depth. Finally, in contrast to some techniques such as X-ray diffraction, the VISIR and LIBS techniques do not require sample preparation.

[3] The May 2000 Field Integrated Design and Operations (FIDO) and K9 Mars prototype rover field trials near Black Rock Summit, Nevada [*Arvidson et al.*, 2002] was the first occasion during which a LIBS instrument was integrated onto a rover test bed and cross-calibrated with a reflectance spectrometer in a field setting (Figures 1 and 2). Specifically, the LIBS field prototype was installed on the mast-head and within the body of the K9 scout rover (Figures 3 and 4). The K9 rover was to scout ahead and identify targets from which the FIDO sampling rover would make detailed measurements and acquire drill cores. IR reflectance data were acquired using the FIDO sampling rover both during the joint rover tests and during unilateral FIDO operations designed to rehearse selected aspects of the MER Missions. VISIR reflectance spectra were also acquired using a ground-based commercial instrument not on either rover and on a regional scale from Airborne Visible and Infrared Imaging Spectrometer (AVIRIS) data covering the site. Unfortunately, owing to time constraints and extenuating circumstances (the devastating wildfire at Los Alamos that prevented LIBS personnel from attending the field tests), only a small amount of LIBS data was taken in the field with K9, and these observations were not calibrated. Even so, key elemental signatures could be

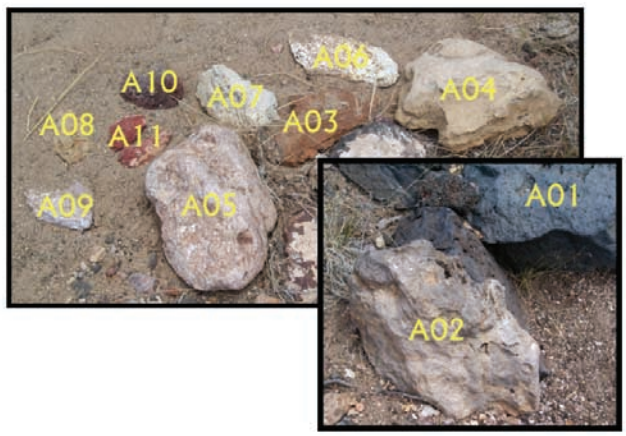

Figure 2. Eleven of the fourteen samples measured in the field with both the laser-induced breakdown spectroscopy (LIBS) and reflectance instruments. The samples were located in the arroyo rover test site indicated in Figure 1. Sample A05 is ~20 cm long.

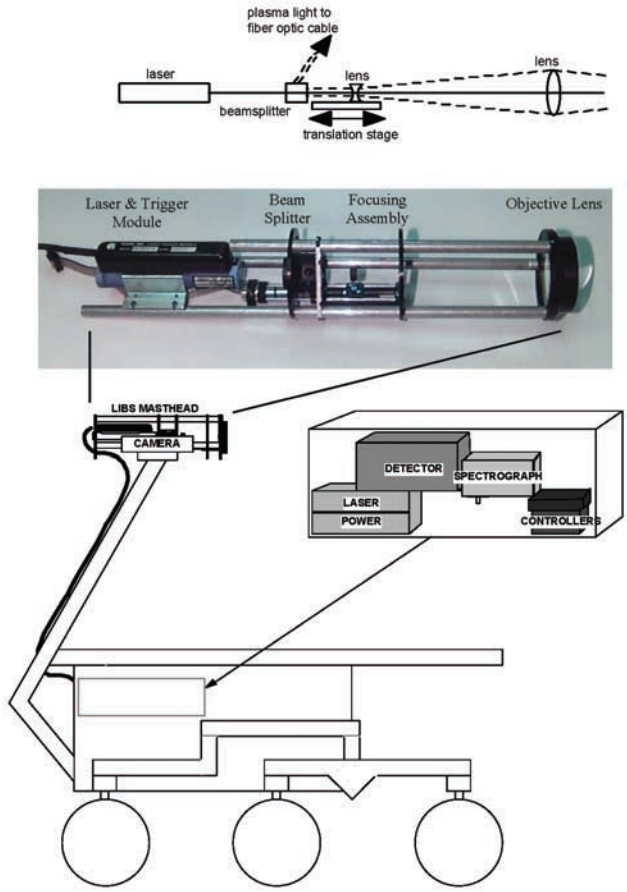

Figure 3. Layout of the LIBS instrument on the K9 rover. The cover of the sensor head is removed to show the internal components. A fiber optic cable carries the collected plasma light to the spectrograph and detector in the body of the rover.

Figure 4. The K9 rover in the field. The LIBS sensor head can be seen mounted on the right side of the mast head instrument suite. The range finder (not shown in Figure 3) is seen as a protrusion to the right of the LIBS sensor head. Photo courtesy of NASA Ames Research Center.

easily discerned. A more substantial cross comparison of VISIR and LIBS data was done in the laboratory using key samples collected from the field site. In this article we report the laboratory results and discuss the synergy between VISIR and LIBS techniques, as well as how the two techniques can be used to the best advantage during future rover missions. We also discuss the added importance of hand specimen descriptions of the type that could be derived from mast-based imaging coupled with arm-based, close-up imaging.

2. Instrumentation

2.1. Imaging

[4] Samples were imaged in the field and in the laboratory using an array of digital cameras. Further, in the laboratory, samples were examined by eye and with a 10× hand lens to simulate what will be done with the close-up imager to be flown on the MER mission.

2.2. Reflectance Spectrometer

[5] An Analytical Spectral Devices (ASD) FieldSpec Pro Full Range portable reflectance spectrometer was used at the field site to acquire data during traverses in order to understand the spectral and lithologic variety of materials exposed at the site. Key samples were then collected for subsequent laboratory data acquisition. The ASD instrument has a spectral range of 0.35–2.5 μm and a spectral resolution of 3 nm at 0.7 and 10 nm at 2.1 μm. Data were acquired in the field from a stand-off distance of ∼2 m and in the laboratory from a range of ∼0.5 m, both using 1 degree field-of-view fore-optic. The spot diameter ranged from 3.5 cm for the 2-m stand-off measurements down to <1 centimeter for the laboratory data.

2.3. Laser-Induced Breakdown Spectrometer

[6] The LIBS technique utilizes a laser pulse to atomize and excite material from a target up to several meters away [e.g., *Cremers and Radziemski*, 1986]. The excited atoms emit at characteristic wavelengths in the near ultraviolet and visible spectral regions, producing a visible spark. The light from the spark is collected and spectrally analyzed. Emission lines from the laser-induced spark are characterized by sharp peaks of ∼0.1-nm full-width, half-maximum. Nearly all elements have strong peaks between 180 and 850 nm. Because of the short duration and limited spatial extent of the plasma, the spectral background is negligible in all cases.

[7] The applicability of LIBS to space exploration was first discussed some time ago [*Blacic et al.*, 1992]. Recent work has shown that the LIBS technique works well at pressures from one bar down to a vacuum [*Knight et al.*, 2000]. As a function of decreasing pressure, the emission intensity rises strongly, reaching a peak roughly 10 times stronger at ∼100 torr pressure, before dropping off slowly, equaling terrestrial atmospheric intensity at 0.1 torr and dropping slightly further in a complete vacuum. For Martian atmospheric pressures between 4 and 8 torr, intensities are several times greater than those observed at terrestrial atmospheric pressure. The intensity variations are due to (1) the expansion speed of the plasma, such that in a complete vacuum the plasma is poorly confined, so that emission occurs over a large volume, (2) reduced collisions as the pressure is decreased, thereby reducing the number of reexcitations of atomic species per unit time, and (3) the change in mass of target ablated per laser pulse. The ablated mass increases steeply between terrestrial atmospheric pressure and ∼100 torr due to a significant decrease in shielding of the target by the laser plasma at lower pressures.

[8] In a series of tests conducted with targets in a simulated Martian atmosphere of 5–10 torr CO_2, using a very compact 35 mJ Nd:YAG laser at 19-m distance, detection limits for nearly all elements were found to be in the range of 2–700 ppm. The measurement accuracy and precision of rock powder samples were found to be 10–12% and 5–7%, respectively, for most of the major elements, based on soil and stream sediment standards [*Knight et al.*, 1999]. In addition, dust layers of 1-, 2-, and 3-mm thickness were completely removed using 4, 14, and 28 laser pulses, respectively. (The nonlinear scaling likely resulted from some dust falling back into the hole, which was created by directing the beam vertically down onto a horizontal surface.) Depth profiling through highly consolidated samples such as basalt occurs at much slower rates of ∼1 μm/pulse [*Knight et al.*, 2000]. Depth profiling through ∼100 μm thick Mn-rich desert varnishes has also been demonstrated.

[9] The LIBS field instrument used for our tests consists of two sections: the sensor head, which was mounted on the rover mast, and the body, mounted inside the body of the rover (Figure 3). The sensor head consists of optical transmission and acquisition systems, as well as a range

finder (visible in Figure 4). The optical transmission system consists of the laser, filter, and a beam expander. The compact flash lamp-pumped Nd:YAG laser (Figure 3) produces pulses of 10-ns duration and ~85-mJ energy at 1064 nm. The laser trigger module is comounted in the sensor head. The laser repetition rate is limited by cooling requirements to 0.1 Hz. The 7× beam expander consists of a diverging lens mounted on a linear programmable translation stage and a 50-mm-diameter antireflection-coated objective lens. The same beam expander is used in the optical acquisition subsystem. A beam splitter is used to divert a fraction of the returning plasma light to the fiber optic cable that carries the signal to the spectrograph and detector in the rover body. A glan-focault prism was originally used, allowing 50% of the returning light to be collected with no loss to the outgoing laser intensity. However, concerns about possible changes in polarization of the laser output at higher temperatures in the desert resulted in using a simple quartz plate beam splitter with some loss of light collection.

[10] The rover body houses the spectrograph and detector as well as the laser power supply. The spectrograph contains two 2400 line per mm gratings with blaze angles of 250 and 500 nm. The detector consists of an intensified CCD detector. Each spectrum recorded with this system covers a range of ~80 nm, with resolution limited to ~1 nm by the spectrograph. The working spectral range is from 250 to ~750 nm. The lower-wavelength cutoff is caused by transmission losses in the beam expander optics. At wavelengths above 500 nm, second-order features begin to be seen. These can be removed by insertion of a short-wavelength blocking filter. The upper end of the spectrum is limited by stray light from the laser flash lamp, which causes increasing interference above ~700 nm.

[11] The sensor head (Figure 3), with its cover, weighs ~800 g. The instrument has an effective working range of 2–6 m. The closer distance is limited by the height of the sensor head from the ground and the restricted angle of tilt of the pan-and-tilt mechanism on which the LIBS sensor was mounted at the top of the rover mast, a little over 1.8 m above ground level. The maximum distance is limited by the ability to generate a strong plasma and to collect sufficient plasma light under terrestrial atmospheric conditions. Operation to ~10 m was achieved in the laboratory using the glan-focault prism. Note that in the Martian environment the instrument would have significantly higher signal/noise because of the greater plasma intensities at Martian atmospheric pressures.

[12] In the field the LIBS instrument was operated by first aiming at one of the samples, which was accomplished with the K9 rover masthead pan-and-tilt mechanism using bore-sighted cameras to confirm the position. The range finder was activated to determine the target distance, and the lens was moved to achieve sufficient laser power density on the target to produce a plasma. The laser beam spot size on the target was typically 1 mm. The laser was then pulsed at 10-s intervals. Single spectra could be obtained or multiple spectra could be averaged to increase the signal-to-noise ratio. If other spectral ranges were desired, the grating was moved and additional spectra were taken. The LIBS instrument was controlled through a computer linked to the rover. In the laboratory, LIBS was used as a stand-alone system at a distance of 2 m. The LIBS field data consisted of a single cleaning pulse followed by a single measurement pulse for each spectral range. Preliminary qualitative field data were given by *Seelos et al.* [2000]. While these were sufficient for identification of the rock type in cases where weathering coatings were minimal, it is greatly preferred to use an average of several pulses taken following several cleaning pulses, as was performed for data taken subsequently in the laboratory. It was also found that field spectra in the short-wavelength range (e.g., $\lambda < 350$ nm) had unusually low signal/noise, possibly owing to misalignment, which would have been corrected in a normal field operation. The only significant difference between field and laboratory spectra is the number of averaged shots. The LIBS data shown in this article were taken in the laboratory and consist of averages of 10 or 20 shots, several shots below the surface unless otherwise stated.

[13] Generally, no attempt was made to check compositional variations encountered during a sequence of shots except near the sample surfaces, as will be discussed later. Laboratory data were taken for all 14 rock samples in the range of 250–340 nm. Additional data were taken for some samples in the ~370–460 nm range, while a few samples were analyzed at higher spectral ranges, such as to check for the presence of hydrogen, indicating bound water or water in surface coatings. Many of the major elements are present in the ranges sampled. Notably absent from these ranges, however, are C, Na, and K. A carbon line at 247 nm is just below the UV cutoff for the prototype LIBS instrument but should be obtainable with improved optics. Very prominent peaks of sodium and potassium occur at higher wavelengths. A flight instrument should have easy access to the whole spectral range to enable analyses of these important elements. Significant improvements in spectral range and resolution made on the prototype subsequent to this field work will be discussed in a forthcoming article.

[14] The LIBS results discussed in this article are qualitative in nature, aimed at elucidating the mineralogy without giving exact elemental compositions. While LIBS is certainly capable of yielding quantitative results within approximately ±10% accuracies [e.g., *Knight et al.*, 1999; 2000], the present setup did not lend itself well for this. The spectrograph used in these tests was of relatively low resolution of $\lambda/\Delta\lambda \sim 350$, which potentially allowed interfering peaks to go unrecognized. For example, the strong aluminum peak seen at ~309 nm is actually a double peak, with minor Ti peaks both in between the two peaks and slightly to the lower wavelength side of the peaks. Additional Al peaks at 393 and 397 nm have interferences from strong neighboring Ca lines at this resolution. Some of the other elements have similar potential interferences. Additionally, the rocks analyzed in these tests had a large compositional range varying from typical basalt to limestone and dolomite, to highly enriched alteration products including goethite, kaolinite, and high-silica replacement. Calibration tests were carried out with 16 rock powder standards from sources including the USGS, NBS, etc. The standards were analyzed in the laboratory under the same conditions as the rocks. A

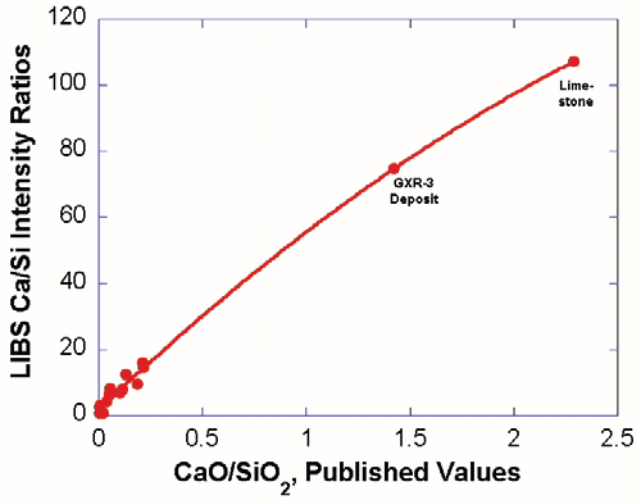

Figure 5. LIBS calibration curve for Ca/Si. Data were taken in the laboratory using rock powder standards of known composition compiled by *Govindaraju* [1994]. The curve is a quadratic fit to the data with a correlation coefficient of 0.998.

calibration curve for Ca/Si is shown in Figure 5. Calibrations were done as ratios rather than individual element absolute intensities so that they would be applicable regardless of the sample-to-instrument distance or the efficiency of creating a plasma on a given surface. For Figure 5, peak intensities at the wavelengths of 393.4 and 390.5 nm were used, respectively, for Ca and Si. As can be seen in Figure 5, calibrations are non-linear in nature, thus requiring more data points than a linear response. The mean error for standards plotted on this curve is 22%, which drops rapidly if low-Ca standards are excluded, with a mean error of 13% for $CaO/SiO_2 > 0.06$. As will be seen below, the LIBS data proved very useful in understanding the samples in tandem with VISIR despite the qualitative nature of the results given here.

3. Results

[15] We report here laboratory-based results for the 14 samples collected from the field site. LIBS results were obtained by qualitative comparisons with the database of standards mentioned above. The compositions of LIBS standards shown in the figures are given in Table 1. Elemental compositions for the rocks were estimated by qualitative comparisons with these and other standards. For VISIR data, spectral features characteristic of end-member minerals and phases were identified through comparison to the USGS spectral library [*Clark et al.*, 1993, available at http://speclab.cr.usgs.gov] in both the normalized reflectance and continuum-removed domains. A numerical linear unmixing routine was also used to identify primary end-member phases. On the basis of the hand specimen examination there are four major rock types in the sample suite: basalt, iron oxides, altered rhyolite, and dolostone. Representative VISIR spectra for each rock type are presented in Figure 6a–d. LIBS spectra are shown in the figures that follow. A summary of the findings for each sample is given in Table 2. Details of each rock type are discussed below.

3.1. Basalt

[16] In hand specimen, both samples (A01 and A10) exhibit aphanitic, vesicular textures, typical of extrusive basaltic materials. Sample A01 is dark gray with visible olivine aggregates up to 4 mm in diameter and relatively unaltered except for discontinuous bright coatings of fine particulate matter. Sample A10 is dark reddish-purple with no discernable mineral crystals, prominent flow banding, and abundant vesicles infilled with fine-grained bright material.

[17] The continuum removed VISIR reflectance spectrum for sample A01 (Figure 6a) shows evidence for fayalitic olivine, based on the broad extent of the 1.060-μm absorption feature [*Hunt and Salisbury*, 1970]. The absorptions located at 1.414 and 1.908 μm indicate the presence of hydroxyl (OH^-) and molecular water, respectively [*Clark et al.*, 1990]. The feature located at 2.205 μm matches the cation-hydroxl (Al-OH) bending mode typical of montmorillonite [*Hunt and Salisbury*, 1970]. The overall spectrum is consistent with an olivine normative basalt with a montmorillonite-bearing coating [e.g., *Israel et al.*, 1997]. The low reflectivity of the basalt sample and the associated subtleness of the spectral features brought about the need to perform the analysis in the continuum-removed domain. This undermined the possibility of performing numerical unmixing on the spectral data set.

[18] LIBS spectra for A01, shown in Figure 7a and 7b over the ranges 250–340 and 370–460 nm, respectively, are similar in appearance to spectra of the basalt rock powder standard, the spectra of which are shown directly below the sample. The 250–340 nm region (Figure 7a) shows prominent peaks for Fe, Mg, Si, Al, Ca, and Ti. The 370–460 nm region (Figure 7b) includes prominent Si, Mg, Ca, and Fe peaks. Tables 1 and 3 give the published composition of the standard and the whole-rock XRF composition of the sample, respectively. Notable differences are the higher Mg and Ti and lower Si in the sample as compared to the standard. In the elemental abundance ranking for A01 in Table 2, iron is ranked higher than aluminum because of the higher peak at 323 nm relative to

Table 1. Major Element Compositions of Rock Powder Standards[a]

	JB-2 Basalt	NBS-88b Dolomite	IF-G Iron Form	NIM-G Granite
SiO_2	53.20	1.13	41.20	75.70
Al_2O_3	14.67	0.36	0.15	12.08
Fe_2O_3	3.13		37.20	0.58
FeO	10.09		16.78	1.30
MnO	0.20	0.02	0.04	0.02
MgO	4.66	21.03	1.89	0.06
CaO	9.89	30.12	1.55	0.78
Na_2O	2.03	0.03	0.03	3.36
K_2O	0.42	0.10	0.01	4.99
TiO_2	1.19	0.02	0.01	0.09
P_2O_5	0.10	0.00	0.06	0.01
H_2O	0.38	0.24	0.47	0.49
CO_2		46.67	0.30	0.10
Fe_2O_3T	14.34	0.28	55.85	2.02
Total	101.08	100.00	101.57	99.70

[a] From *Govindaraju* [1994] for which LIBS Spectra are shown in the figures.

Table 2. Summary of Rock Characteristics Based on Hand Specimen, Reflectance, and LIBS Results

Sample	Hand Specimen Descriptions	Spectral Analysis Results	Analysis Spots	LIBS Elemental Abundance Ranking (averaged over all spot analyses)						Primary LIBS Descriptions	LIBS Accessories and Surface Features
				SiO_2	Al_2O_3	Fe_2O_3	MgO	CaO	TiO_2		
A01	Vesicular basalt; rare olivine aggregates in fine-grained groundmass	fayalitic basalt with clay mineral coating	2	1	3	2	5	4	6	basaltic	very thin clay surface layer (Al-, H-rich)
A02	Cataclastic texture, reddish and grey vein-filling material; dust coating	dolomite with iron oxide and kaolinite	4	3	4	5	2	1	6	dolomitic	occasional thick kaolinitic coverings
A03	Banded reddish-brown, fine-grained with quartz clasts; minor fine-grained dust	goethite, partially altered to limonite	4	1–2	3	1–2	4			Iron-rich	
A04	Crystalline texture, minor reddish material in fractures; bright dust coating	dolomite with iron oxide and kaolinite	2	2	4–5	4–5	3	1	6	dolomitic	very thin Si-, Al-, Ti-rich layer
A05	Altered porphyritic rhyolite; former feldspar, quartz, and dark mineral; bright coating	kaolinite and goethite	6	1	2	3	4–5	4–5	6	mainly kaolinitic	a mélange of $CaCO_3$, Fe-rich, and Si-rich regions
A06	Altered rhyolite; massive white clay with brown spots; bright dust coating	kaolinite and iron oxide	5	1	2–4	5	2–4	2–4	6	kaolinitic-dolomitic	1 spot Mg-, Ca-rich, with some Si, Al; 1 spot dolomite with Fe
A07	Altered porphyritic rhyolite; former feldspar, quartz, dark phase, and glass; dust coating	kaolinite and iron oxide	3	1	2	3	5	4	6	kaolinitic	constant Al, Mg, Si; varying Ca, Fe, Ti
A08	Altered porphyritic rhyolite; former feldspar, quartz, biotite, and glass; dust coating	kaolinite and iron oxide	3	1	2	3	5	4	6	mainly kaolinitic	1 spot kaolinite; 1 spot kaolinite with Fe, Ti; 1 spot $CaCO_3$
A09	Altered porphyritic rhyolite; former feldspar, quartz in fine-grained groundmass; dust coating	kaolinite and iron oxide	3	1	2	3	5	4	6	Al-rich, also Mg, Ca, Fe, Si	1 spot Fe-rich
A10	Vesicular basalt; reddish-purple, fine-grained with flow banding; bright dust coating	altered basalt with hematite, goethite, clay coating	3	1	3	2	5	4	6	basaltic	
A11 A14	Finely banded reddish material and silica, occasional quartz grains; bright dust coating	iron oxide with minor carbonate	5	1	2	3	4	5	6	silica- and iron-rich	whitish coating is $CaCO_3$; 2 spots Si-rich; 1 spot Fe-rich
A12 A13	Banded fine-grained reddish material and silica with occasional quartz grains; minor dust	goethite with hydrated silica	6	1	3	2	4	5	6	Silica- and Iron-rich	thin Fe-rich surface coating; 2 spots Fe-rich; 4 spots Si-rich

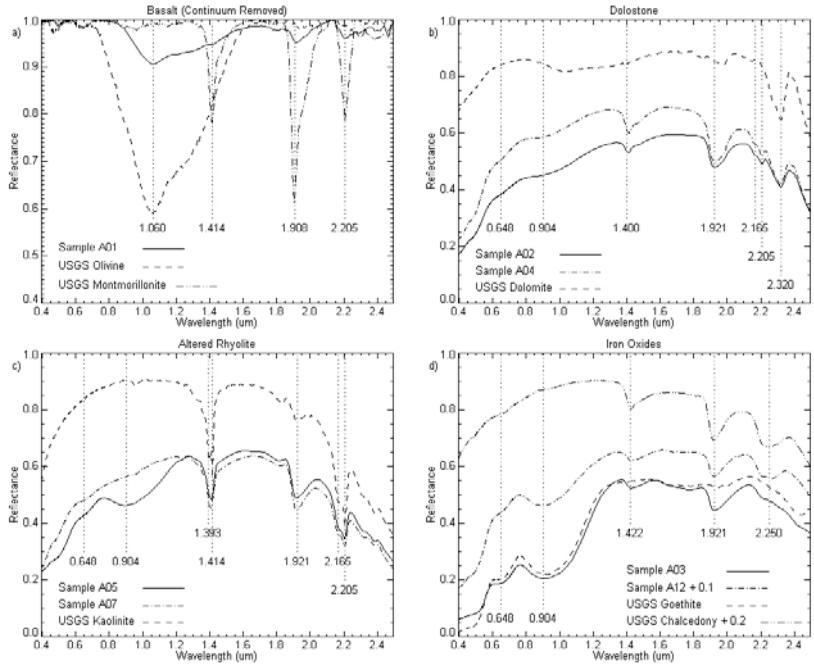

Figure 6. Reflectance spectra for samples of basalt, dolomite, rhyolite altered to kaolinite, and iron oxide, with lab spectra for comparison.

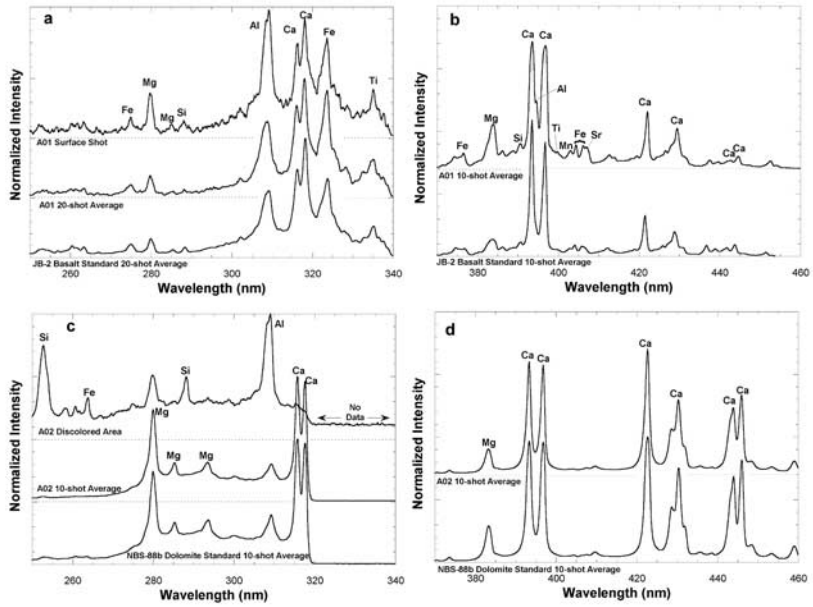

Figure 7. LIBS spectra of (a, b) basalt and (c, d) dolostone for the spectral ranges from 250–340 and 370–460 nm, taken in the laboratory. Figure 7a and 7b compare the basalt standard, JB-2 (Table 1) with sample A01. The bottom two spectra in Figure 7a and both spectra in Figure 7b show the standard and the A01 20-shot average taken after 10 cleaning shots. The top spectrum in Figure 7a shows the distinct Al-, Mg-, Si-rich surface layer. In Figure 7b the broader 393- and 397-nm Ca peaks in the A01 spectrum compared to the standard suggests these peaks are saturated, resulting in relatively higher minor peaks in the A01 spectrum. Figure 7c and 7d show the NBS-88b dolomite standard as the bottom spectra, with the 10-shot average of dolomitic sample A02, taken after cleaning shots, directly above the standard. The top spectrum in Figure 7c shows a discolored area of A02, located several millimeters from the first spot, which has a significantly different composition. Ca lines at 393 and 397 nm are saturated in Figure 7d. In Figure 7c the 318-nm Ca lines are normally stronger than the 316-nm Ca lines (cf. Figure 7a) but are slightly truncated due to being near the edge of the useable spectrum.

Table 3. X-ray Fluorescence Compositions of the Four Rock Types

	A01 Basalt	A02 Dolostone	A03 Fe Oxides	A04 Dolostone	A05 Altered Rhyolites	A07 Altered Rhyolites
SiO_2	44.33	3.93	56.05	1.30	72.61	80.93
TiO_2	2.88	0.05	0.06	0.04	0.62	0.39
Al_2O_3	15.36	0.85	1.04	0.79	15.01	12.45
Fe_2O_3	14.65	0.44	27.82	0.06	2.05	0.12
MnO	0.20	0.02	0.01	0.01	0.01	0.00
MgO	8.55	15.86	0.84	15.88	0.23	0.16
CaO	9.12	33.96	4.76	35.79	1.86	0.45
Na_2O	3.37	0.01	0.27	−0.01	0.12	0.21
K_2O	1.14	0.03	0.23	0.05	0.15	0.10
P_2O_5	0.50	0.04	0.19	0.03	0.14	0.03
LOI[a]	−0.32	44.51	8.42	45.88	6.94	5.06
Total	99.77	99.70	99.69	99.81	99.76	99.90

[a] LOI, loss on ignition. Negative loss on ignition indicates gain on ignition, usually owing to oxidation of FeO.

the standard. While the two LIBS analysis spots may well have had a higher iron abundance, the XRF whole-rock data (Table 3) shows an iron abundance just slightly (0.7%) below that of aluminum.

[19] Evidence for a montmorillonite surface coating suggested by VISIR data was not initially seen in LIBS data taken in the normal mode of first performing several cleaning shots. However, by analyzing the surface shots instead of discarding the data it became clear that there was a very thin coating enriched in Al, Mg, and Ti. The top spectrum in Figure 7a shows these features for an initial surface shot, which are clearly distinct from the lower two spectra characteristic of basalts. By the third pulse the features in the top curve had dropped to their normal amplitudes seen in the middle curve, suggesting that the alteration coating was either very thin or very loosely adhering.

[20] LIBS has the important capability of detecting hydrogen via the 656-nm emission line, and this can be used to distinguish hydrated minerals. Bound water, as seen in the VISIR spectrum of A01 (Figure 6a), is not expected for a basaltic composition, and hydrogen abundances indicative of hydration were not seen initially by LIBS when the cleaning-shot data were discarded. However, subsequent investigation of the initial surface shots showed significant hydrogen that was rapidly removed. Figure 8 shows the H peak for the first, third, and fifth shots, as well as for multiple shots taken well below the surface for both A01, the basalt, and A07, which is a kaolinitic sample as discussed below. The hydrogen emission line is unique in that it is the only elemental line to be strongly broadened by the Stark effect [*Griem*, 1974]. For A01, Figure 8 clearly shows a significant hydrogen component in the initial shot, which dropped rapidly by the third shot. For a further comparison of A01 a saw cut surface was analyzed. The H peak for its initial shot was just above the A01 third shot and well below the first shot in Figure 8. This is further proof that the alteration features seen by VISIR on sample A01 were very tenuous and easily removed by LIBS. In contrast, the hydrogen peak in the kaolinitic sample (A07) did not drop between the first and third shots, and the "deep" multiple-shot spectrum shows a hydrogen peak nearly as large as the A01 initial shot plotted in the lower half of Figure 8.

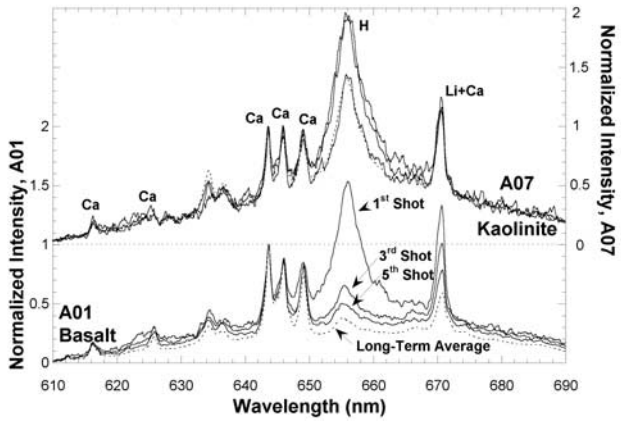

Figure 8. LIBS spectra of samples A01 (a basalt) and A07 (a kaolinitic sample) in the spectral range showing hydrogen, taken in the laboratory. All spectra are normalized to the peak of the 643-nm Ca line = 1.00. For each sample, single-shot spectra are shown of the first, third, and fifth shots, as well as a multiple-shot average taken well below the surface. In each case, the H peak was highest for the initial shot and progressively dropped.

3.2. Dolostone

[21] Representatives of this category include samples A02 and A04. A02 is gray to brown and shows cataclastic texture as well as veins filled with reddish and gray fine-grained materials. A04 is light beige with only minor red coatings. On the basis of visual examination a favored interpretation for these samples would be that of a carbonate rock which has been modified by either soft sediment deformation or cataclastic processes.

[22] The reflectance data for samples A02 and A04 (Figure 6d) display several distinctive features, including a dolomite combination band at 2.320 μm [*Gaffey*, 1987], the characteristic 2.2-μm kaolinite doublet, and multiple Fe^{3+} charge transfer features associated with iron oxide phases (discussed in greater detail below). These spectral characteristics suggest the samples have dolomite, kaolinite, and goethite present on their surfaces, although the linear unmixing routine assigned dolomite the largest fractional abundance for both samples with 15 and 21% weight for samples A02 and A04, respectively.

[23] LIBS data from A02 show Ca and Mg are high in abundance relative to all other measured elements. Figure 7c and 7d compares a dolomite standard with a 10-shot average from A02 taken after a number of cleaning shots,

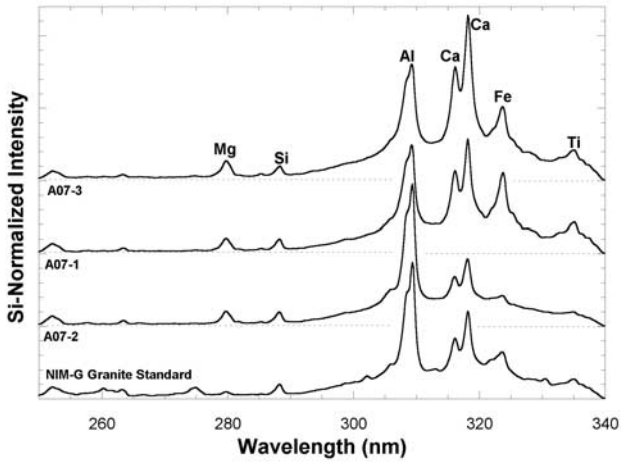

Figure 9. LIBS spectra in the 250–340 nm range for three different analysis spots of sample A07, typical of the altered rhyolite. The curves are normalized to the 288-nm Si peak.

shown over nearly the same ranges as for the basalts in Figure 7a and 7b. Owing to its high sensitivity, there is still a noticeable Al peak in the lower two curves in Figure 7c even though the Al_2O_3 abundances are <1% (Tables 1 and 3). The top curve in Figure 7c shows the spectrum of a more reddish spot located several millimeters away from the first location. This curve shows that Ca is almost nonexistent, whereas Si and Al are high at this location, consistent with the presence of kaolinite (cf. Figure 9). There are also traces of iron and magnesium. Further analysis showed that some areas contained thin coverings, rich in Si + Al and/or Fe, that were removed within ~10 shots, while other, relatively rare areas, had macroscopically thick Si + Al-rich patches adhering to the dolostone. Thus the combination of data show that A02 is primarily dolomite but includes representative materials exposed in many areas in and around the rover test site.

[24] Sample A04 was also identified by LIBS as dolomitic in composition, very similar to A02. The compositions of the analysis spots are within the range for analysis spots on A02. Analysis of the very surface, in this case the first three shots, shows additions of Al, Si, Fe, and Ti as surficial contaminants.

3.3. Altered Rhyolites

[25] Several rock samples collected from the field site (A05–A09) are a type of altered rhyolite. This conclusion was drawn based on visual determination of an aphanitic-porphyritic texture, abundant feldspar, low abundance of dark minerals, and both granular and interstitial quartz. The degree of alteration varies from sample to sample, but in all cases the feldspars are completely altered, and the dark mineral phase is often represented by only a rust-colored stain. For example, sample A06 has been completely altered into a soft, massive white rock with occasional brown spots. On the other hand, samples A08 and A09 are relatively pristine with only the larger feldspar phenocrysts showing any effects of alteration. Samples A05 and A07 are intermediate examples. The observed extent of alteration could in part be due to compositional variations since feldspar is the most readily weathered mineral in the assemblage. All samples have visible patches of bright dust coatings, concentrated in pits and low areas.

[26] The spectral reflectance data for samples A05 and A07 (Figure 6c) have both sets of doublet features indicative of kaolinite. These doublets are centered near 1.4 and 2.2 μm and are the result of hydroxyl stretch overtones and an Al-OH bending mode plus hydroxyl stretch combination [*Clark et al.*, 1990]. Both samples show strong evidence for molecular water in the form of a band near 1.9 μm and a muting of the 1.4 μm doublet by a water combination band. While the linear unmixing routine identified kaolinite as a major component in both samples (22 and 45% for samples A05 and A07, respectively), sample A05 was also assigned a goethite component at the 34% level. Spectrally, this is justified by the characteristic ferric ridge and band minima locations in the visible and near-infrared region.

[27] LIBS analyses of sample A07 appeared high in Al, clearly consistent with the VISIR kaolinite identification. Figure 9 shows spectra in the 250–340 nm range for three different analysis spots on A07, as well as a granite standard (Table 1) for comparison. Note the variations in Ca, Fe, and Ti abundances between the three analysis spots. The clay-like nature was further identified by the persistence of a significant hydrogen peak regardless of depth below the surface, as already discussed in connection with Figure 8.

[28] Sample A05 was very heterogeneous on the surface and to the depths sampled by LIBS. Six different spots were analyzed by LIBS. Spectra in the 250–340 nm range are shown in Figure 10, normalized to maxima of 1.0. Spot 1 is nearly pure SiO_2 (assuming other major elements such as K and Na are also nearly absent), with only traces of Al, Fe, and Ti. Spot 2 is a low-Ca, high-Al silicate, most likely kaolinite. Spot 3 is similar to spot 2 but has a higher Ca content. Spot 4 is also similar but has higher iron. Spot 5 is nearly pure $CaCO_3$ (the C is assumed). Spot 6 is mostly $CaCO_3$, with some Al, Mg, Si but very little Fe, Ti. The preponderance of analysis spots favor a high aluminum silicate composition, consistent with kaolinite, but clearly show how heterogeneous a heavily weathered rock can be.

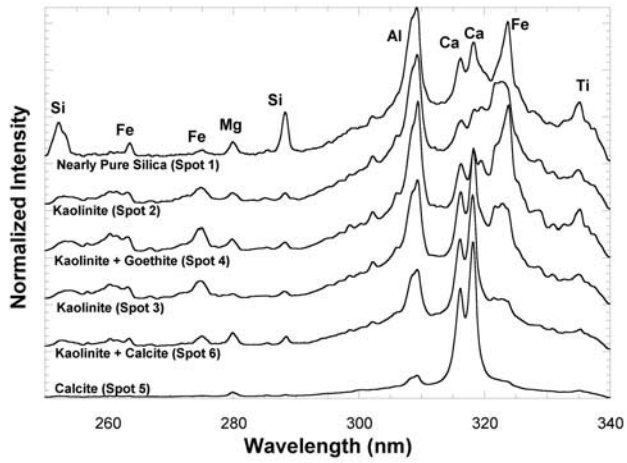

Figure 10. LIBS laboratory spectra of sample A05 showing the large range of compositions encountered at six different spots on the sample. Each spectrum is normalized to the highest peak.

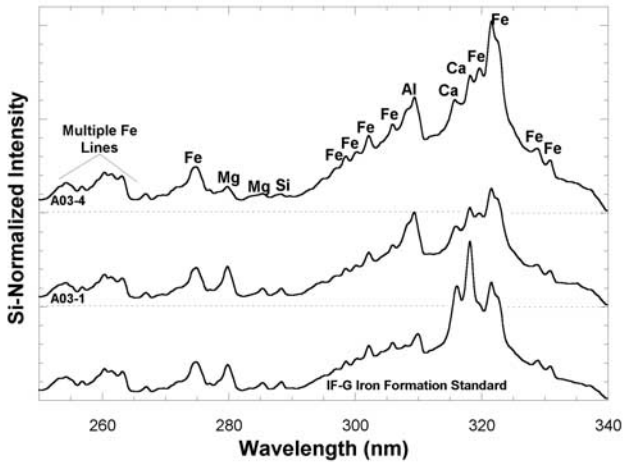

Figure 11. LIBS laboratory spectra for two analysis spots on sample A03, and an iron formation standard, all showing high-iron compositions. The numerous minor iron peaks contribute to an apparent high background.

VISIR and LIBS are in agreement that this sample is very heterogeneous, the added identification of high silica and pure $CaCO_3$ coming from LIBS.

3.4. Iron Oxides

[29] The fourth type of rock collected at the field site includes samples A03 and A11–A14 and consists of finely banded to massive dark reddish-orange material with occasional bands or grains of what appears to be glass or chalcedony. Relatively little accumulation of dust is observed on the surface of these samples.

[30] The spectral reflectance linear unmixing routine reported goethite at >70% abundance for sample A03 (Figure 6b). This interpretation is corroborated by the presence of the ferric iron ridge in the visible and near-infrared wavelengths and by the exact location of the band minima (0.648 and 0.904 μm) in this spectral region [*Morris et al.*, 1985]. The band minima locations for sample A12 also have the best correspondence to those of goethite, as opposed to other iron-oxide phases with Fe^{+3} crystal field spectral bands. As is the case with the basaltic spectral data, hydroxyl and water molecules are manifest in the form of spectral features in the 1.4- and 1.9-μm regions. The linear unmixing routine indicated a nonnegligible cryptocrystalline SiO_2 component for sample A12. This can be seen in the spectral data as a broad feature at 2.250 μm attributable to an Si-OH vibrational absorption [*Graetsch et al.*, 1985].

[31] LIBS spectra of sample A03 (Figure 11) show that this sample is very high in iron, and because iron has numerous peaks, both weak and strong, the background appears high at this low spectral resolution. The relatively weak silicon line at 288 nm is still visible, indicating that Si is still present. Titanium is below the detection limit, while the visible 280-nm Mg peak suggests the presence of some Mg. The strong lines of Al and Ca are still visible but are suggestive of roughly 1% and subpercent levels, respectively.

[32] For sample A12 three of the four spots analyzed showed very high silica compositions, as shown for the 20-shot average in Figure 12. Available silicon emission lines are relatively weak, so that while the observed Si lines in Figure 12 are not the highest intensity peaks, comparison with other compositions suggests the spots analyzed on A12 are nearly pure SiO_2. For example, the intensity of the Si line relative to Al, Ca, Fe, Ti, and Mg is significantly higher in A12 than in any of our rock powder standards, including standards for granite (77% SiO_2) and sandstone (90% SiO_2). If this composition were observed only for a single spot on a relatively unweathered rock, it could be attributed to a single quartz crystal, particularly, given the small spot size for LIBS analyses. However, in this context, appearing in multiple spots in a heavily weathered environment, the high silica composition is assumed to be an alteration product.

3.5. Summary

[33] Table 2 gives a summary of the results based on the combination of visual examination, VISIR, and LIBS. Analysis of additional samples not mentioned above all fell into the same four rock types, but with varying degrees of heterogeneity. For example, sample A06 was initially identified as kaolinite by VISIR, but most of the analysis spots covered by LIBS appeared to be dolomitic. By contrast, sample A08 likewise appeared kaolinitic by its high Al and Si features. However, one of the three spots analyzed by LIBS showed only Ca in the spectral range analyzed, inferred to be $CaCO_3$. Sample A09 was also Al-rich but had greater variations among Si, Mg, Ca, and Fe. One spot appeared to be very high in Fe. Sample A10 was basaltic, with LIBS spectra similar to A01 and the basalt standard in Figure 7. Samples A11 and A14 were separate pieces of the same rock, as were A12–A13. All four of these showed very high silica composition in some spots and high iron composition in other spots.

[34] On the basis of qualitative comparison of LIBS spectra with the 16 standards, a ranking of elemental abundances was produced covering Si, Al, Fe, Mg, Ca,

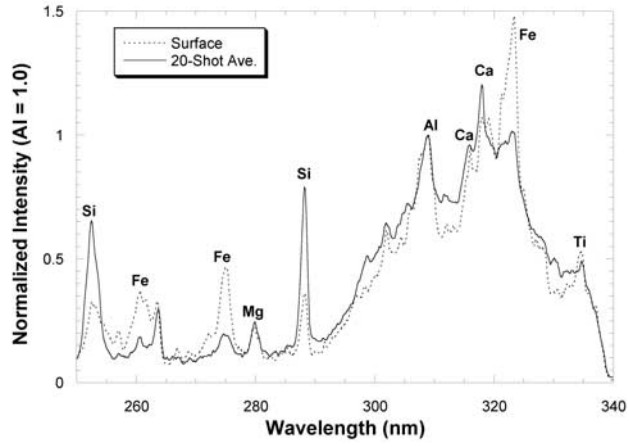

Figure 12. LIBS spectra of sample A12 showing the top three shots (dashed line) and a 20-shot average taken just below the three shots (solid line) on the same spot, taken in the laboratory. Both spectra were normalized to the 309-nm Al peak = 1.0. The three-shot spectrum shows a strongly Fe-enriched surface coating. The 20-shot average shows an almost pure silica composition.

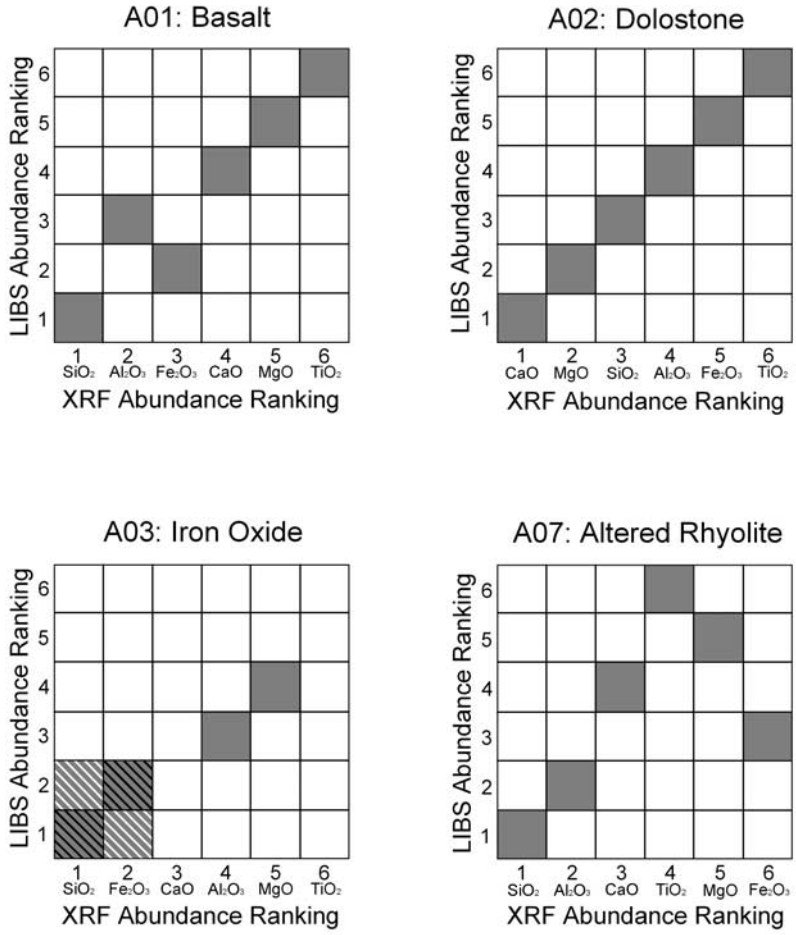

Figure 13. Comparisons of elemental abundance rankings between an average of the LIBS analysis spots for each sample and an XRF whole rock analysis. For sample A03 two of the four LIBS spots gave higher Si and the remaining two spots gave higher Fe. Ti was below the detection limit owing to a high background from numerous low-intensity iron peaks. Ca abundance was not ranked because it was below the comparison standards. For A07, abundances for all but SiO_2 and Al_2O_3 were below 0.5% and spatially variable.

and Ti, all from the 250–340 nm spectral range. This ranking is shown in Table 2 and is also compared for several samples with whole rock XRF data (Table 3) in Figure 13. For the most part the abundance rankings are in very good agreement. Given the low resolution of the LIBS spectrograph, interferences might account for some minor element discrepancies. However, the major reason for differences is more likely sample heterogeneity. For example, for the iron oxide sample A03 two of the LIBS analysis spots gave higher SiO_2 abundances and two gave higher Fe_2O_3 abundances. This "whole-rock ambiguity" is shown in Figure 13 by the cross-hatched area over both SiO_2 and Fe_2O_3. For the altered rhyolite sample A07 the higher ranking by XRF of CaO and MgO are likely due to the XRF measurement containing a larger fraction of dolomite, while the LIBS ranking is based more on kaolinite. Note also that the three spectra of A07 shown in Figure 9 vary widely in abundances. XRF data in Table 3 show that for A07 everything but SiO_2 and Al_2O_3 is below 0.5% abundance, making the ranking of these low-abundance elements largely irrelevant. Surface features also likely explain the Fe-Al swap in the basalt (A01) comparison (according to the XRF results, Al_2O_3 is just 0.7% higher in abundance than Fe_2O_3). In this respect, Figure 13 illustrates the difficulty of determining whole-rock abundances from millimeter-size near-surface analysis spots. For samples with significant heterogeneity, such as in the case of heavy weathering, a bulk technique such as XRF analyses of large portions of samples is the only way to obtain a truly representative bulk composition. However, in this environment, where the degree and type of alteration vary significantly from one portion of the rock to another, a true bulk composition is actually less desirable than to understand the constituent components, which is best done with multiple small-spot analyses.

4. Discussion and Conclusions: Implications for Future Rover Missions and Traverse Science

[35] Work reported in this article was a first attempt at field work and subsequent follow-up laboratory work for LIBS using a prototype of the size and weight approaching

Table 4. Comparison of LIBS and APXS General Characteristics

Parameter	LIBS	APXS
Typical detection limits	2–1000 ppm (element dependent), includes H; poor detection of oxygen, noble gases	≥5000 ppm; cannot detect H, He
Analysis depth	1 μm (basalt) to 250 μm (sand, dust) per pulse; repetitive pulses can depth-profile several mm	~10 μm; surface coatings or dust layers can be problematic; needs RAT
Sampling diameter	~1 mm/shot; whole rock compositions can be obtained by averaging shots over a larger area	~40 mm
Measurement times	10 s/shot with prototype; several minutes for averaging many shots	several hours minimum
Analysis distance	up to 20 m	must be adjacent to sample
Sample acquisition times	determined by speed of rover masthead positioning, focusing. Rover travel not needed for samples within ~20 m	determined by rover travel time to new sample and positioning of sensor head-on sample
Effect of atmospheric gases	intensity varies with total pressure; 5–10 torr ~3× higher signal than 1 bar; elemental ratios unchanged	presence of CO_2 complicates data interpretation
Mass and power	≤2.5 kg; <5 W expected for flight instrument	0.6 kg; 1.5 W

LIBS information based on *Knight et al.* [1999, 2000]; APXS information based on *Reider et al.*[1997, 2000].

that suitable for use on a Mars mission, and a first attempt to synergistically use LIBS and VISIR to characterize a suite of rocks. Several limitations prevented this investigation from being quantitative in terms of elemental compositions. Among them were the large range of compositions encountered at this site, from nearly pure silica to nearly pure $CaCO_3$ to dolomite and more typical clay and basaltic compositions. This was combined with the low spectral resolution and limited spectral range of the current spectrograph. In terms of the LIBS instrument development this work represents a snapshot in time, as our currently upgraded prototype instrument now has been greatly expanded in both spectral range and resolution (D. Cremers, manuscript in preparation, 2002). The state of the art continues to advance rapidly in this area, so that conventional spectrographs of the same size and mass can now provide expanded range and higher resolution. In addition, very compact echelle spectrographs are now in the size range that might be considered for use on a rover.

[36] The work reported here was very useful in understanding the utility of LIBS even in a qualitative sense and even using only a small portion of the available spectrum. As a potential new technique for planetary geology, it is important to understand the advantages and disadvantages of, for example, the ~1-mm spot size used by remote LIBS. This work shows that while single spot analyses may not be representative of the bulk rock, analysis of several spots rapidly converges on an accurate characterization of the rock. Another interesting feature is the ability of LIBS to distinguish surface coatings that passive techniques tend to report as admixtures with the bulk rock. Differences in interpretation between LIBS and VISIR tended to be due to surface coatings. Plots showing surface and bulk rock differences are shown for LIBS for samples A01, A02, and A12 (Figures 7, 8, and 12). Clearly, these surface coatings make a difference in field work on Earth, and the differences are expected to be more so on Mars, where dust coatings are ubiquitous. LIBS would be expected to identify actual end-members where other instruments would tend to show mixtures, such as the mixtures with global dust composition seen by Pathfinder.

[37] Another distinct advantage of LIBS over present techniques is the identification of relative abundances of hydrogen. Figure 8 shows the broad hydrogen peak for both a hydrated clay and a terrestrial basaltic rock. No measurement has yet been made of hydrogen abundances in soils or rocks on Mars. It is likely that no exposed surfaces are hydrated at the surface or to depths (e.g., up to a couple millimeters) that LIBS could depth profile into a sample. However, LIBS could be very important as a tool to use with subsurface drilling, either through an optical fiber down the borehole or on cores brought to the surface, or simply to investigate under rocks moved, e.g., by the rover. Given the priority of characterizing the presence and history of water on Mars, this capability is important. Figure 8 also points out another important feature of LIBS, and that is the low detection limits for a number of minor and trace elements. At the spectrograph resolution used here the very strong 671-nm Li line blends together with a 672-nm Ca line in Figure 8. However, at reasonable spectral resolutions these are easily distinguished. LIBS has a very low detection limit for lithium, at several parts per million. There are a number of elements with detection limits below 50 ppm, such that their relative abundances can be assessed in most rocks. Minor or trace elements typically seen in many to most rocks when using a higher resolution spectrograph and larger spectral range include Li, F, Sr, Ba, V, Cu, and Cr.

[38] An important feature of the present LIBS and VISIR analyses is that the analyses of all 14 rocks took on the order of only a few hours. For a long-range rover the time required for each analysis will be critical in achieving a complete characterization of the surroundings while also covering a significant average distance per sol. The ability to make remote measurements and the time required for each measurement are both important in achieving rapid characterization. The LIBS prototype described here compiled 10-shot averaged spectra in 100 s. The flash lamp-pumped laser was limited to 0.1 Hz. Expense kept us from

obtaining and using a diode-pumped laser of the type expected for a flight instrument. These are far more efficient and are presently in routine use in laser altimeters. A LIBS flight instrument with a diode-pumped laser would likely operate a factor of 10 or more faster than the prototype for the same amount of power. This would decrease analysis times below their already short durations and also allow significantly greater depth profiling within samples. Operating lifetimes of these lasers are in the millions, if not billions, of shots. Testing of susceptibility to dust, as will be encountered on Mars, also indicates that a flight LIBS instrument should be very robust. LIBS data can be collected equally well, though at reduced signal intensities, with the objective lens covered with dust to such a degree that the overall transmission is significantly reduced (D. Cremers, manuscript in preparation, 2002).

[39] Table 4 summarizes some of the advantages of LIBS by comparing characteristics with APXS, which was used on the Sojourner rover and is planned for MER-A and MER-B in 2003. Table 4 covers a number of important areas affecting the comprehensiveness of the data, speed and ease of analysis, and susceptibility to complications by dust, weathering layers, or atmospheric constituents.

[40] The Martian surface covers a large area, at nearly 150 million km^2. The exploration strategy up to now has been to use orbiting spacecraft to determine large-scale differences on the surface and to use rovers to provide in situ measurement for a few rocks and soils around a landing site. However, a huge gap remains between the content or "depth" of information from orbital data and the areal coverage of the presently planned rovers and their payloads. Long-range rovers, beyond the 1-km traverses planned for MER-A and MER-B will eventually be part of the exploration program. These systems will need long-surface lifetimes, faster travel capabilities, and the ability to acquire mineralogical and elemental composition data remotely. Remote analysis capabilities are important, not only because they are key to the decreased analysis times needed for ground-based analytical coverage of large areas but also to access areas not available for in situ analysis. Some of the most interesting areas may include cliff faces with exposed stratigraphic layering and other tantalizing features [e.g., *Malin and Edgett*, 2000]. Vertical or near-vertical cliff faces and embankments are completely out of reach of in situ rover instruments. Remote instruments operating from the rover would greatly extend the capabilities of a rover in rough terrain and at the bottoms of exposed cliffs. This would be particularly true if selected samples also could be examined using close-up imaging to delineate textures.

[41] This work shows the distinct advantages of combining three remote-sensing techniques for rapid rover-based characterization, potentially useful for long traverses. The key databases are (1) visual information of rock texture, (2) mineralogical information, and (3) elemental composition. Visual information is important to understand the origin of the samples. In the samples described here, textural information was key to understanding that the samples with kaolinitic mineralogical and elemental signatures were in fact altered rhyolite. Mineralogical information is obviously important even if elemental composition is available. The VISIR measurements highlighted here tended to overemphasize the clay compositions over low-reflectivity compositions such as the basalt. Other remote mineralogical techniques, such as thermal emission [e.g., *Christensen et al.*, 2000] or remote Raman spectroscopy [*Lucey et al.*, 1998, *Wiens et al.*, 2000], each have respective advantages and disadvantages, which will not be discussed here. For elemental compositions, LIBS is the only technique to offer remote measurements. The elemental data give a clearer understanding of the composition and origin of samples than can be determined by mineralogical techniques alone by distinguishing between different elemental end-members within mineral groups. In summary, we expect that the combination of these three databases (visual, elemental, and mineralogical, all of which can be obtained rapidly at remote distances) to be key to future rover exploration of Mars.

[42] **Acknowledgments.** This work is supported by the NASA Mars Instrument Development Program through contract W-19,460. REA and FS were supported through NASA Planetary Geology and Geophysics Program through grant NAG5-7830 from the Goddard Space Flight Center. The authors wish to thank NASA Ames personnel (including H. Thomas, M. Bualat, A. Wright, L. Kobayashi, and K. Bass) for assistance with integration of the LIBS instrument on the rover, and for assistance in obtaining LIBS data in the field. Assistance and advice were also provided by J. Nordholt, H. Newsom, D. Vaniman, and W. Calvin. We thank N. Snider for figure production and background work and R. Couture for XRF analyses. Helpful reviews by N. Izenberg and one anonymous reviewer were greatly appreciated.

References

Arvidson, R. E., S. W. Squyres, E. T. Baumgartner, P. S. Schenker, C. S. Niebur, K. W. Larsen, F. P. Seelos IV, N. O. Snider, and B. L. Jolliff, FIDO prototype Mars rover field trials, Black Rock Summit, Nevada, as test of the ability of robotic mobility systems to conduct field science, *J. Geophys. Res.*, *107*(E9), 10.1029/2000JE001464, 2002.

Blacic, J. D., D. R. Petit, D. A. Cremers, and N. Roessler, Laser-induced breakdown spectroscopy for remote elemental analysis of planetary surfaces, *Proc. Int. Symp. Spectral Sens.*, 302–312, 1992.

Christensen, P. R., G. L. Mehall, N. Gorelick, S. Silverman, and the Athena Science Team, The Athena Miniature Thermal Emission Spectrometer (Mini-TES), in *Concepts and Approaches for Mars Exploration*, pp. 67–68, *LPI Contrib.1062*, Lunar and Planet. Inst., Houston, Tex., 2000.

Clark, R. N., V. V. Trude, M. K. King, and G. A. Swayze, High spectral resolution reflectance spectroscopy of minerals, *J. Geophys. Res.*, *95*, 12,653–12,680, 1990.

Clark, R. N., G. A. Swayze, A. J. Gallagher, T. V. V. King, and W. M. Calvin, The U.S. Geological Survey, Digital Spectral Library: Version 1: 0.2 to 3.0 microns, *U.S. Geol. Surv. Open File Rep.*, *93–592*, 1340 pp., 1993.

Cremers, D. A., and L. J. Radziemski, Laser plasmas for chemical analysis, in *Laser Spectroscopy and Its Applications*, edited by L. J. Radziemski, R. W. Solarz, and J. A. Paisner, chap. 5, Marcel Dekker, New York, 1986.

Gaffey, S. J., Spectral reflectance of carbonate minerals in the visible and near infrared (0.35–2.55 μm): Anhydrous carbonate minerals, *J. Geophys. Res.*, *92*, 1429–1440, 1987.

Golombek, M. P., R. A. Cook, T. Economou, W. M. Folkner, A. F. C. Haldemann, P. H. Kallemeyn, J. M. Knudsen, R. M. Manning, H. J. Moore, and T. J. Parker, Overview of the Mars Pathfinder Mission and assessment of landing site predictions, *Science*, *278*, 1743–1748, 1997.

Govindaraju, K., Compilation of working values and sample description for 383 geostandards, *Geostand. Newsl.*, *18*, 1–158, 1994.

Graetsch, H., O. W. Flörke, and G. Miehe, The nature of water in chalcedony and opal-C from Brazilian agate geodes, *Phys. Chem. Miner.*, *12*, 300–306, 1985.

Griem, H. R., *Spectral Line Broadening by Plasmas*, Academic, San Diego, Calif., 1974.

Hunt, G. R., and J. W. Salisbury, Visible and near-infrared spectra of minerals and rocks, I, Silicate minerals, *Mod. Geol.*, *1*, 283–300, 1970.

Israel, E. J., R. E. Arvidson, A. Wang, J. D. Pasteris, and B. L. Jolliff, Laser Raman spectroscopy of varnished basalt and implications for in situ measurements of Martian rocks, *J. Geophys. Res.*, *102*, 28,705–28,716, 1997.

Knight, A. K., D. A. Cremers, M. J. Ferris, N. L. Scherbarth, R. C. Wiens, J. D. Blacic, W. M. Calvin, and J. E. Nordholt, Development of a pro-

totype instrument for stand-off elemental analysis for use on a Mars rover, in *Fifth Int. Conf. on Mars*, pp. 6064–6065, Lunar and Planet. Inst., Houston, Tex., 1999.

Knight, A. K., N. L. Scherbarth, D. A. Cremers, and M. J. Ferris, Characterization of laser-induced breakdown spectroscopy (LIBS) for application to space exploration, *Appl. Spectrosc.*, *54*, 331–340, 2000.

Lucey, P. G., T. F. Cooney, and S. K. Sharma, A remote Raman analysis system for planetary landers, *Lunar Planet. Sci.*, *XXIX* 1354–1355, 1998.

Malin, M. C., and K. S. Edgett, Evidence for recent groundwater seepage and surface runoff on Mars, *Science*, *288*, 2330–2335, 2000.

McSween, H. Y., S. L. Murchie, J. A. Crisp, N. T. Bridges, R. C. Anderson, J. F. Bell, D. T. Britt, J. Bruckner, G. Dreibus, T. Economou, and A. Ghosh, Chemical, multispectral, and textural constraints on the composition and origin of rocks at the Mars Pathfinder landing site, *J. Geophys. Res.*, *104*, 8679 –8715, 1999.

Morris, R. V., H. V. Lauer, C. A. Lawson, E. K. Gibson, G. A. Nance, and C. Stewart, Spectral and other physiochemical properties of submicron powders of hematite, maghemite, magnetite, goethite, and lepidocrocite, *J. Geophys. Res.*, *90*, 3126–3144, 1985.

Reider, R., T. Economou, H. Wänke, A. Turkevich, J. Crisp, J. Brückner, G. Dreibus, and H. Y. McSween, The chemical composition of Martian soil and rocks returned by the mobile alpha proton x-ray spectrometer: Preliminary results from the x-ray mode, *Science*, *278*, 1771–1774, 1997.

Reider, R., J. Brückner, G. Klingelhöfer, R. Gellert, G. Dreibus, G. Lugmair, H. Wänke, and the Athena Science Team, The Athena alpha proton x-ray spectrometer (APXS), in *Concepts and Approaches for Mars Exploration*, *LPI Contrib.1062*, pp. 267–268, Lunar and Planet. Instit., Houston, Tex., 2000.

Seelos, F. P., R. C. Wiens, D. A. Cremers, M. Ferris, J. D. Blacic and R. E. Arvidson, Combined remote mineralogical and elemental measurements from rovers, in *Concepts and Approaches for Mars Exploration*, *LPI Contrib. 1062*, pp. 279–280, Lunar and Planet. Instit., Houston, Tex., 2000.

Wiens, R. C., D. A. Cremers, M. Ferris, J. E. Nordholt, J. D. Blacic, P. Lucey, and S. K. Sharma, Development of a prototype laser-induced breakdown spectroscopy (LIBS) instrument with stand-off Raman capabilities as part of the Mars Instrument Development Program, *Lunar Planet. Sci.*, *XXXI*, 1468–1469, 2000.

R. E. Arvidson, K. S. Deal, and F. P. Seelos IV, Department of Earth and Planetary Sciences, McDonnell Center for the Space Sciences, Washington University, St. Louis, MO 63130, USA.

J. D. Blacic, Earth and Environmental Sciences, Los Alamos National Laboratory, Los Alamos, NM 87545, USA.

D. A. Cremers and M. J. Ferris, Chemistry Division, Los Alamos National Laboratory, Los Alamos, NM 87545, USA.

R. C. Wiens, Space and Atmospheric Sciences, NIS-1, MS D-466, Los Alamos National Laboratory, Los Alamos, NM 87545, USA. (rwiens@lanl.gov)